# An Ultrafast Optoelectronic THz Beam System:

## Applications to Time-Domain Spectroscopy

**BY D. GRISCHKOWSKY**

Recently, there has been a great deal of work demonstrating the generation of THz radiation (1 THz = 33.3 $cm^{-1}$ = 4.1 meV) via material and electronic excitation by ultrashort laser pulses. Modern integrated circuit techniques have made possible the precise fabrication of micron-sized dipoles, which, when photoconductively driven by fsec laser pulses, can radiate well into the THz regime.[1,2] An alternative and complimentary approach has been to extend radio and microwave techniques into the THz regime through the use of optoelectronic antennas.[3-11] Other sources based on various physical systems and effects include the emission of an electromagnetic shock wave due to a volume dipole distribution moving faster than the phase velocity in the medium, *i.e.*, electro-optic Cherenkov radiation,[12,13] and the electromagnetic shock wave radiated by a surface-dipole distribution propagating faster than the phase velocity in the substrate.[14,15]

Most recently, radiation has been generated by photoconductively driving the surface field of semiconductors,[16,17] of strained layer superlattices,[18] and the intrinsic region of a silicon p-i-n diode[19] with ultrafast laser pulses. Another new and quite efficient source of broadband THz radiation involves the generation of photocarriers in trap-enhanced electric fields with ultrafast laser pulses.[20,21]

Some of these sources are based on an optical type approach whereby a transient point source of THz radiation is located at the focus of a dielectric collimating lens, followed by an additional paraboloidal focusing and collimating mirror. [2,8,10,20] This type of source, developed by my group, produces well collimated beams of THz radiation. Matched to an identical receiver, the resulting system has extremely high collection efficiency. With a demonstrated signal-to-noise ratio of 1000, a time resolution of less than 150 fsec, and a frequency range from 0.2 THz to more than 5 THz, this optoelectronic THz system is presently the most highly developed and will be the one described in this article.

A high-performance optoelectronic source chip, used to generate pulses of freely propagating THz electromagnetic radiation, is shown in Figure 1a.[20] The simple coplanar transmission line structure of the chip consists of two 10 μm wide metal lines separated by 80 μm fabricated on high-resistivity GaAs. Irradiating the metal-semiconductor interface (edge) of the positively biased line with focused ultrafast laser pulses produces synchronous bursts of THz radiation. This occurs because each laser pulse creates a spot of photocarriers in a region of extremely high electric field. [21] The consequent acceleration of the carriers generates the burst of radiation. A colliding-pulse modelocked (CPM) dye laser provides the 623 nm, 60 fsec excitation pulses at a 100 MHz repetition rate in a beam with an average power of 5 mW at the 10 μm diameter excitation spot. The major fraction of the laser generated burst of THz radiation is emitted into the GaAs substrate in a cone normal to the interface and is then collected and collimated by a crystalline silicon lens attached to the back side of the chip.

The teraHz optics[8,10] used in the complete optoelectronic

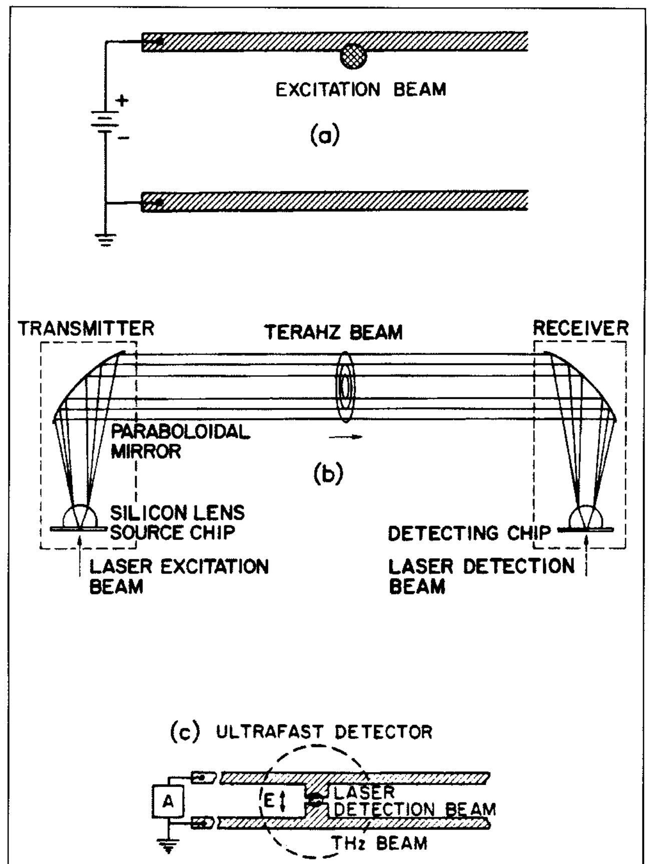


FIGURE 1. (a) Configuration used to generate the freely propagating pulses of THz radiation. (b) THz collimating and focusing optics. (c) Receiving antenna geometry.

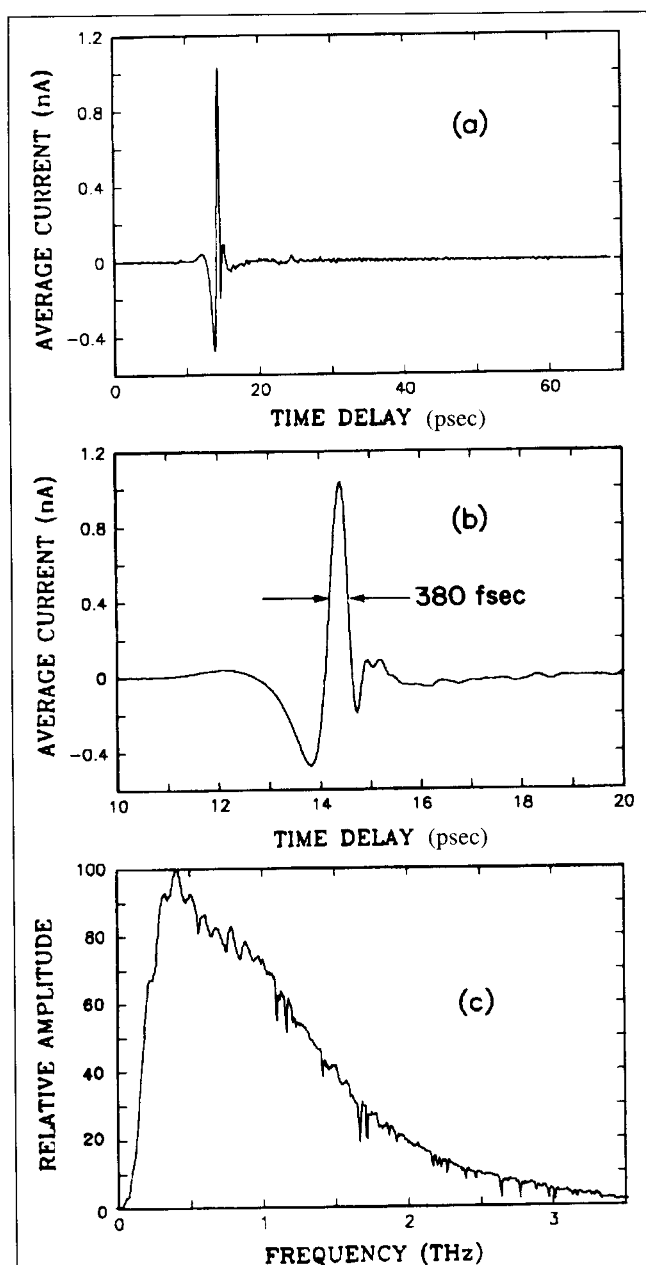


FIGURE 2. (a) MEASURED THZ PULSE TO 70 PSEC. (b) MEASURED THZ PULSE ON AN EXPANDED 10 PSEC TIME SCALE. (c) AMPLITUDE SPECTRUM TO 3.5 THZ OF THE THZ PULSE OF FIGURE 2A.

system are illustrated in Figure 1b. They consist of two matched crystalline silicon lenses, one contacted to the back side of the GaAs source chip and the other to the silicon-on-sapphire (SOS) detection chip. Each lens is located near the foci of two identical paraboloidal mirrors. The combination of the silicon lens and the paraboloidal mirror collimates the emitted radiation to beam diameters proportional to the wavelength and with a frequency-independent divergence of typically 25 mrad. The second identical combination on the receiving end focuses the teraHz beam on the detector. The entire system is located in an airtight enclosure to mitigate the effects of water vapor on the THz beams.[2]

The THz radiation detector is an ion-implanted SOS detection chip with the antenna geometry shown in Figure 1c. The 20-μm-wide antenna structure is embedded in a coplanar transmission line consisting of two parallel 5-μm-wide aluminum lines separated from each other by 10 μm. The electric-field of the focused incoming THz radiation induces a transient bias voltage across the 5 μm gap between the two arms of this receiving antenna, directly connected to a low-noise current amplifier. The amplitude and time dependence of this transient voltage is obtained by measuring the collected charge (average current) versus the time delay between the THz pulses and the CPM laser detection pulses. These pulses in the 5 mW laser detection beam synchronously gate the receiver by driving (closing) the photoconductive switch defined by the 5 μm antenna gap. Simply speaking, the switch is closed by the photocarriers created by the 60 fsec laser pulse; the switch then reopens in approximately 600 fsec due to the short carrier lifetime in ion-implanted SOS.

The measured THz pulse emitted from the laser excited metal-GaAs interface with +60V bias across the transmission line is shown in Figure 2a, and on an expanded time scale in Figure 2b. The measured pulsewidth with no deconvolution is seen to be 380 fsec. At the time these results were obtained,[20] they were the shortest directly measured THz pulses; the dip on the falling edge was the sharpest feature ever observed with an ion-implanted detector and indicated a response time faster than 190 fsec. The numerical Fourier transform of the pulse of Figure 2a, as presented in Figure 2c, extends to beyond 3 THz; the sharp line structure is due to residual water vapor present in the system.

In work (to be presented this month at QELS '92) using this same type source and detector—but with tighter optical focusing, better matched silicon lenses, and with the THz optical system of Figure 1b optimized to have a unity, frequency-independent, transfer function—ultrashort THz pulses were measured with a ringing structure faster than 160 fsec. Their amplitude spectrum peaked at 1 THz; the relative amplitude at 3 THz was 20%, at 4 THz was 5%; useful radiation extended to 5 THz. These results confirm the response time of the receiver to be faster than 150 fsec, in agreement with a direct characterization,[22] and show that the entire optoelectronic system is competitive with the alternative approach of THz interferometry.[23,24]

As required by the reciprocity principle, good receivers are good transmitters. It is possible to use an antenna as illustrated in Figure 1c. for the THz source. This was an early approach and many different combinations of antenna lengths, shapes, and semiconductors—GaAs:As,[25,26] GaAs,[26-29] and ion-implanted SOS[2,8,10,22,30]—have been used. For the THz source chip, the carrier lifetime is of little concern be-

cause the THz radiation is proportional to the time derivative of the current pulse and, therefore, is mainly generated on the steep rising edge. Antenna of the same geometry but with longer arms between more widely separated lines produce stronger, slower pulses with lower peak frequencies.[28]

Different detectors can also be used. Although other materials have been tried,[26] we generally use ion-implanted SOS material due to its reproducible properties and short carrier lifetime. The antenna length is chosen to suit the measurement. The 10 μm-long antenna, shown in Figure 1c, has a relatively flat response from low frequencies to 6 THz and, thereby, does not limit the time resolution of our measurements. In fact, the electrical response is completely determined by the intrinsic response time of the semiconductor, in agreement with the measured 150 fsec time resolution of this detector.[22] Slower, more sensitive antennas are obtained simply by increasing the separation between the coplanar lines, while keeping constant the 5 μm photoconductive gap separation between the two arms. [28]

An alternative method of source characterization, which bypasses the problems of receiver bandwidth, is based on far-infrared interferometric techniques using a power detector. This approach was first demonstrated for THz radiation sources[23] by measuring auto-correlation signals with a fullwidth-at-half-maximum (FWHM) of 230 fsec for the THz radiation pulse from laser created carriers accelerated by the surface field of a photoconductive semiconductor. This approach used a single THz radiation source, illuminated by 10 Hz repetition-rate, amplified, 100 fsec pulses from a CPM dye laser, together with a Martin-Puplett interferometer and a liquid helium cooled bolometer. A different interferometric approach, using unamplified, 100 MHz repetition rate, CPM dye laser pulse excitation of a two source interferometer, has since been demonstrated.[24] Via this approach, together with fast, scanning-delay-line averaging, orders of magnitude improvements in the signal-to-noise ratio of the measured interferograms were obtained. Using this method, the THz radiation source described in Figure 1a was shown to produce radiation to 6 THz. In addition, a 230 fsec FWHM auto-correlation signal and an average power of 30 nW for 4 mW of laser excitation power were measured for this source.[24]

## Time-Domain Spectroscopy

The powerful technique of time-domain spectroscopy (TDS) has recently been applied to several different systems using a variety of sources.[27] With this technique, two electromagnetic pulseshapes are measured, the input pulse and the propagated pulse—the latter having changed shape due to its passage through the sample under study. Consequently, via Fourier analysis of the input and propagated pulses, the frequency dependent absorption and dispersion of the sample can be obtained. The useful frequency range of the method is determined by the initial pulse duration and the time resolution of the detection process. Therefore, with each reduction in the generated electromagnetic pulsewidth and/or the time resolution of detection, there is a corresponding increase in the available frequency range.

The combination of the TDS technique with teraHz beams has some powerful advantages compared to traditional c.w. spectroscopy. First, the detection of the far-infrared radiation is extremely sensitive. Although the energy per THz pulse is very low (0.1 femtoJoule), the 100 MHz repetition rate and the coherent detection measures the electric field of the propagated pulse with a signal-to-noise ratio of about 10,000 for an integration time of 125 msec.[10] In terms of average power, this sensitivity exceeds that of liquid helium cooled bolometers by more than 1000 times. Second, because of the gated and coherent detection, the thermal background—which plagues traditional measurements in this frequency range—is observationally absent.

By comparing time-domain spectroscopy with Fourier transform spectroscopy (FTS), it should be clear that the frequency resolution of the two techniques is similar, since they are both based on a scanning delay line, where to first order the frequency resolution is determined by the reciprocal of the time scan. However, the fact that TDS scans a delay line with a well collimated optical beam does present some experimental advantages. Although for now FTS is superior above 4 THz (133 $cm^{-1}$), the limited power of the radiation sources and the problems with the thermal background favor TDS below 4 THz.

The most serious experimental problem limiting the accuracy of TDS measurements involves the relatively long term changes in the laser pulses and the consequent changes in the input THz pulses. During an experiment, we first measure the input pulse (with no sample in place), then measure the pulse transmitted through the sample, and finally re-measure the input pulse with the sample removed. This sequence is repeated several times to obtain good statistics. Typically, the amplitude spectral ratio of subsequent input pulses varies by ±5% over the frequency spectrum. This variation limits the accuracy of an absorption measurement. In the same manner, the relative phase of subsequent input pulses varies by ±0.05 radians over the same spectrum, and thereby limits the accuracy of the measurements of the index of refraction. Another experimental consideration involves the frequency distribution across the profile of the THz beam, which consists of a series of overlapping discs with diameters proportional to the wavelength. This feature requires that the sample be uniform and be centered in the beam and that an aperture of the same diameter as the sample blocks any THz radiation from going around the sample. The aperture is kept in place for measurement of the input pulse.

We will now describe several different type measurements that illustrate the generality and usefulness of THz-TDS.

## Water Vapor

An early example of THz time-domain spectroscopy was the characterization of water vapor from 0.25-1.5 THz, where the cross-sections of the nine strongest lines were measured

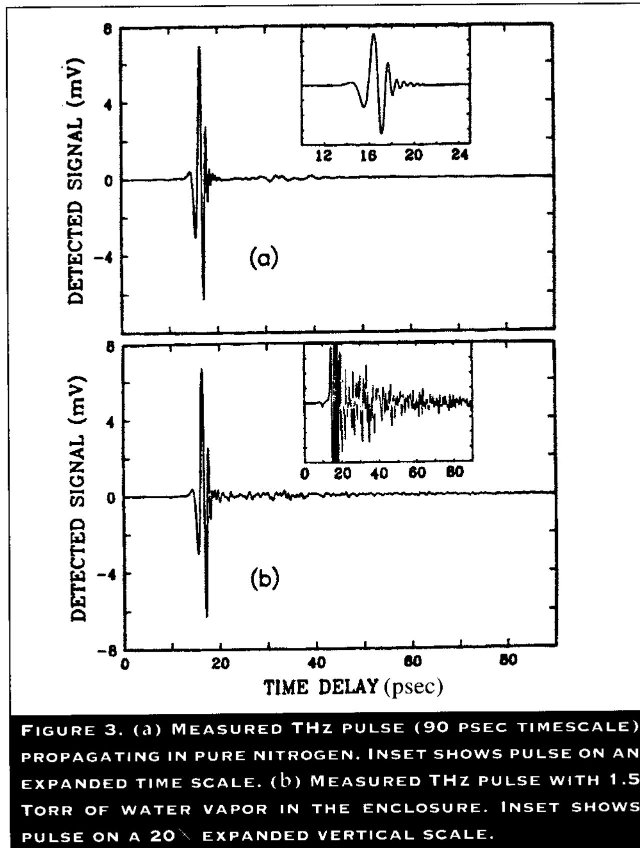


FIGURE 3. (a) MEASURED THz PULSE (90 PSEC TIMESCALE) PROPAGATING IN PURE NITROGEN. INSET SHOWS PULSE ON AN EXPANDED TIME SCALE. (b) MEASURED THz PULSE WITH 1.5 TORR OF WATER VAPOR IN THE ENCLOSURE. INSET SHOWS PULSE ON A 20× EXPANDED VERTICAL SCALE.

with the best accuracy to date.[30] For these measurements, 30 μm long source and detector antennas on ion-implanted SOS substrates were used, together with MgO lenses, instead of the more optimal high-resistivity silicon currently used.

Figure 3a displays the detected teraHz radiation pulses after propagating through pure nitrogen. This measurement was made in a single 10 minute scan of the 200 psec relative time delay between the excitation and detection pulses. When 1.5 Torr of water vapor, corresponding to 8% humidity at 20.5° C, was added to the enclosure, the transmitted pulse changed to that shown in Figure 3b. The additional fast oscillations are caused by the combined action of the dispersion and absorption of the water vapor lines. The slower and more erratic variations seen in both Figures 3a and 3b result from reflections of the main pulse. They are reproducible and divide out in the data analysis. The inset shows the data on a 20× expanded vertical scale. Here, the oscillations are seen to decay approximately exponentially, with an average coherent relaxation time $T_2$.

The amplitude spectra of Figures 3a and 3b are compared in Figure 4a, where the strong water absorption lines are clearly observable. The additional structure on both spectra is not noise, but results from spurious reflections of the main pulse. At each line are indicated the measured frequency with an estimated error of ±0.001 THz and in parenthesis the literature value. The corresponding absorption coefficients are displayed in Figure 4b as the negative of the natural logarithm of the ratio of the two amplitude spectra in Figure 4a. Because the electric field is directly measured, the relative phaseshift between the two spectra is also obtained as plotted in Figure 4c, without the need of the Kramers-Kronig relations. As expected for a Lorentzian line, the magnitude of the jump in phase experienced at each resonance equals the peak absorption.

### SAPPHIRE AND SILICON

The following measurements[27] on single crystal sapphire and silicon were motivated by the need to find the best material for the teraHz lenses in contact with the emitting and detecting chips. The available published data are inadequate for this, and we were forced to perform our own evaluations. Absorption of the THz radiation by the lens material (initially sapphire) imposed an upper limit on the bandwidth of the entire system. The use of silicon lenses, inspired by our measurements of unusually low absorption and dispersion, immediately increased the system bandwidth from 2 to 3 THz and gave smoother THz pulses with less ringing structure.

The single crystal sapphire sample was a polished, 57 mm diameter disc, 9.589 mm thick, and with the C axis in the plane of the disc. A typical THz input pulse incident upon the sample is shown in Figure 5a, and the output pulse (normalized to the input pulse) after propagation through the sample is shown in Figure 5b for which the C axis of the crystal was perpendicular to the polarization. The reduction in amplitude is due to the reflective loss at both surfaces and to the absorption suffered during passage through the sapphire. The pulse at 73.4 psec delay is the ordinary pulse, while the smaller pulse at 85.1 psec delay is the extraordinary pulse. The ratio of the peak of the ordinary pulse to that of the extraordinary pulse is approximately 25:1 and gives the polarization sensitivity of our system.

In terms of amplitude, the polarization ratio of the generated THz beam is 5:1. The 11.8 psec separation between the two pulses is a measure of the birefringence of sapphire and, neglecting the correction to group velocity due to dispersion, directly gives the difference in the index of refraction between the extraordinary and ordinary ray to be $n_e - n_o = 0.37$, compared to the literature value of 0.34.[31,32] When a full frequency analysis is performed, excellent agreement is obtained with the literature value. The 73.4 psec time delay of the ordinary pulse with respect to the 7.1 psec time delay of the pulse with no sample in place gives the ordinary index of refraction $n_o = 3.07$ in agreement with the literature value.[31,32]

The absorption coefficient vs. frequency determined from these pulses is shown in Figure 6a. Here, we see a monotonic increase in absorption with increasing frequency with the expected quadratic dependence. Due to excessive attenuation caused by the sample being too thick for the weak higher frequency components, the data is considered

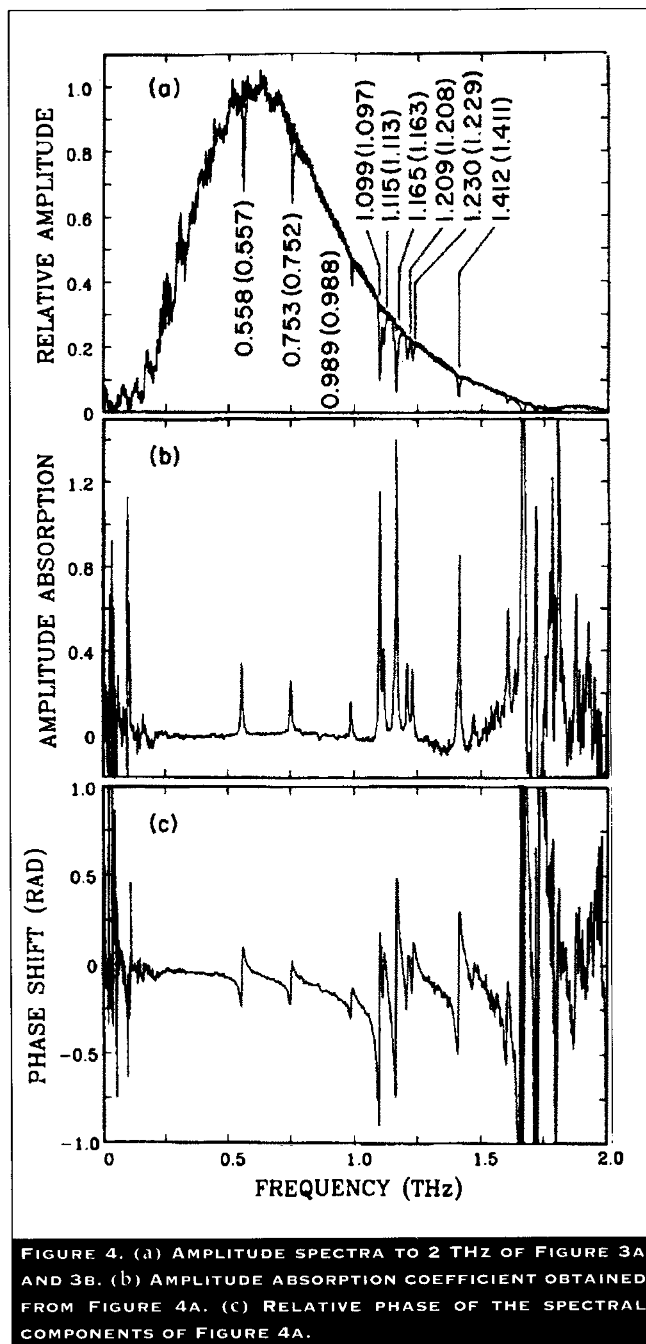


FIGURE 4. (a) AMPLITUDE SPECTRA TO 2 THZ OF FIGURE 3A AND 3B. (b) AMPLITUDE ABSORPTION COEFFICIENT OBTAINED FROM FIGURE 4A. (c) RELATIVE PHASE OF THE SPECTRAL COMPONENTS OF FIGURE 4A.

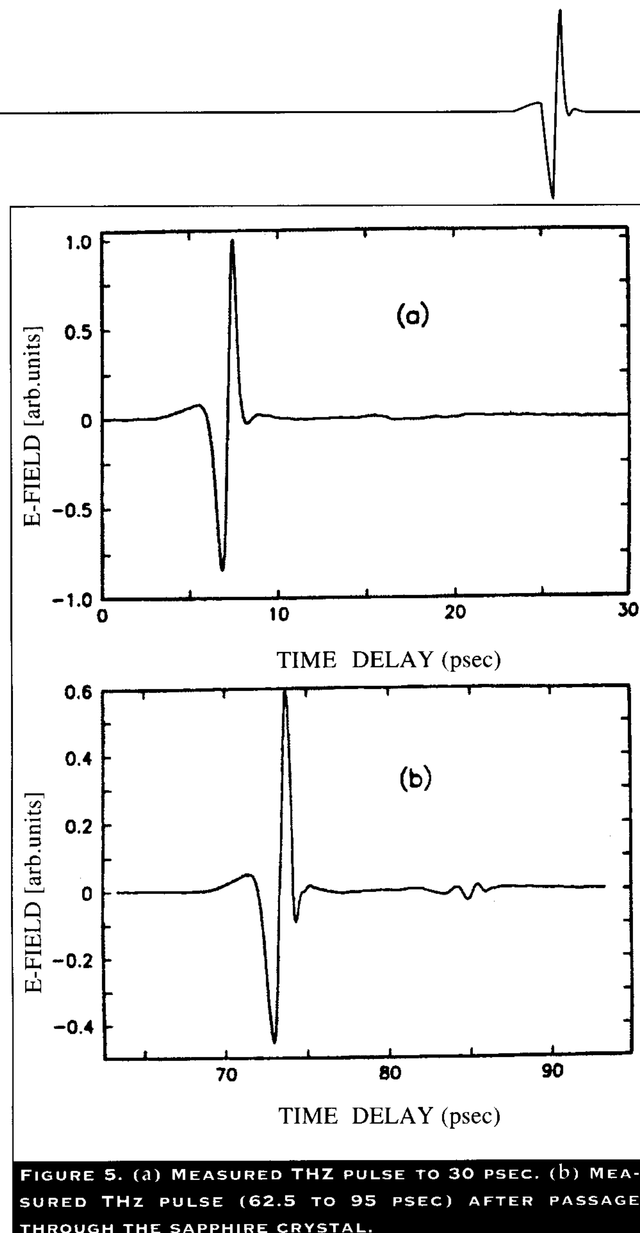


FIGURE 5. (a) MEASURED THZ PULSE TO 30 PSEC. (b) MEASURED THZ PULSE (62.5 TO 95 PSEC) AFTER PASSAGE THROUGH THE SAPPHIRE CRYSTAL.

to be accurate only up to 1.75 THz. Some of the previous work[31-33] has been indicated on the curve and shows a rough agreement (within a factor of 2) with the TDS measurement. The earliest work[31,32] clearly gives too little absorption at low frequencies, where our results are in better agreement with those of Ref. 33. The relative phases of the Fourier components determine the index of refraction vs. frequency as presented in Figure 6b, which compares reasonably well with the indicated earlier results.[31-33]

Crystalline silicon is optically isotropic, eliminating concern about the polarization of the incident THz beam and crystal orientation. Although there is significant literature concerning the far-infrared properties of silicon, below 2 THz there are noteworthy discrepancies among the published data with variations in the measured absorption coefficients of up to 10 times. The main reason for this confusion is that below 2 THz the results are extremely sensitive to the presence of carriers. TDS measurements[28] show that for 1 Ωcm, N-type silicon, the peak absorption is 100 $cm^{-1}$, and that for 10 Ωcm, N-type the absorption is 12 $cm^{-1}$. Extrapolating these values to 100 Ωcm, $\alpha = 1\ cm^{-1}$; at 1 kΩcm, $\alpha = 0.1\ cm^{-1}$, and at 10 kΩcm, $\alpha = 0.01\ cm^{-1}$. Consequently, unless high purity, high-resistivity material is used, what is measured is not the properties of the intrinsic semiconductor but that of the carriers due to residual impurities. This problem is most prevalent in the earlier work on silicon with resistivities of 10 Ωcm [31] to 100 Ωcm.[33]

The following TDS measurements were made on a 50

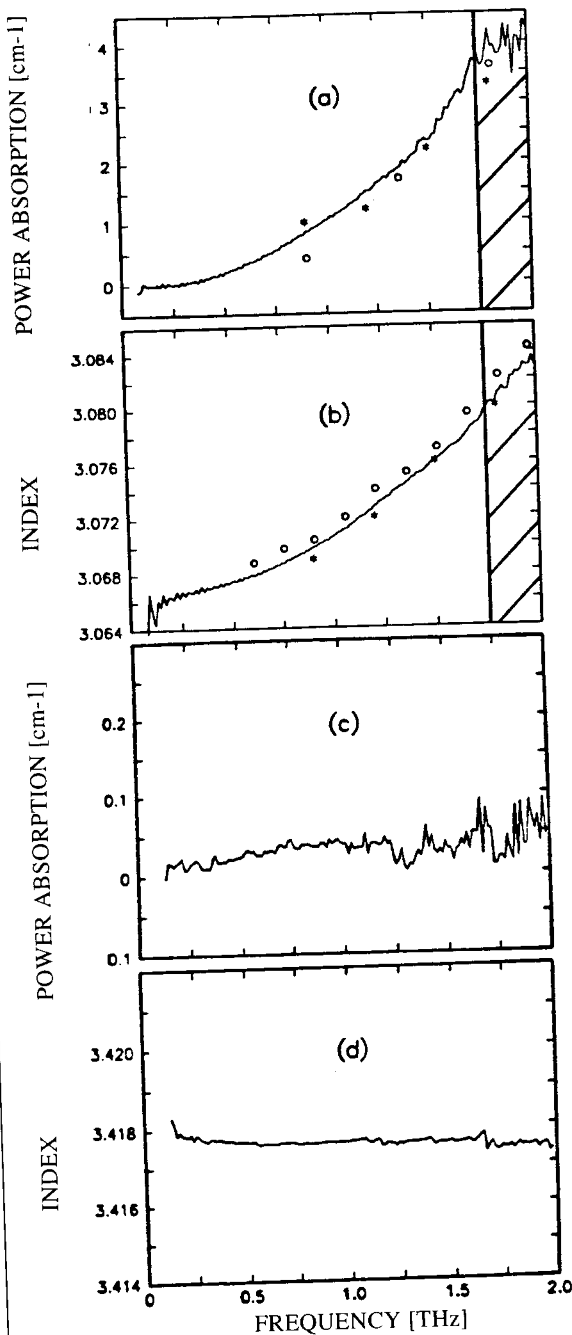


FIGURE 6. TDS MEASUREMENTS TO 2 THZ OF CRYSTALLINE SAPPHIRE AND SILICON. THE CIRCLES ARE THE DATA OF REFS. 31 AND 32: THE ASTERISKS ARE THE DATA OF REF. 33. (a) POWER ABSORPTION COEFFICIENT (ORDINARY RAY) OF SAPPHIRE. (b) INDEX OF REFRACTION (ORDINARY RAY) OF SAPPHIRE. (c) POWER ABSORPTION COEFFICIENT ($CM^{-1}$) OF HIGH-RESISTIVITY SILICON (d) INDEX OF REFRACTION OF HIGH-RESISTIVITY SILICON.

mm diameter, 20.046 mm thick single crystal of high-resistivity (greater than 10 kΩcm), float-zone silicon. For this material, we have measured unprecedented transparency together with a remarkably flat dispersion curve. This is an excellent material for teraHz applications, as can be seen from the absorption spectrum presented in Figure 6c. Throughout the range from low frequencies up to 2 THz, the measured absorption coefficient is less than 0.05 $cm^{-1}$. From the relative phases of the spectral components, the index of refraction vs. frequency is obtained as presented in Figure 6d. Here, the extremely desirable feature of low-dispersion is clearly evident; the index of refraction changes by less than 0.001 over the entire measured spectrum.

## N-TYPE AND P-TYPE SILICON

We now describe a THz time-domain-spectroscopy measurement of the absorption and dispersion due to carriers in device-grade, doped silicon wafers.[28] The frequency-dependent properties were shown to be completely due to the carriers and not to the host crystal. Consequently, the complex conductance could be characterized over the widest frequency range to date. The samples used were a 283 μm thick wafer of 1.15 Ωcm, N-type and a 258 μm thick wafer of 0.92 Ωcm P-type silicon. The measured absorptions shown in Figure 7a are more than 2000 times greater than that of the host crystal. Below 0.15 THz, the data becomes noisy due to the limited beam power, but the theoretically-predicted drop in absorption at low frequencies is clearly observable. The clear difference between the N and P type material is due to the different dynamic behavior of the electrons and holes. For these measurements, the oscillations due to the etalon effects of the sample geometry have been removed numerically. As shown in Figure 7b, the index of refraction is strongly frequency dependent, having a clear minimum followed by a dramatic increase towards lower frequencies. The agreement with the Drude theory (solid line) is exceptional.

As the THz optical properties of the samples are essentially completely determined by the carrier dynamics, the complex electric conductivity of the doped silicon has also been measured. Independent of Drude theory and relying on only very general assumptions,[28] the electric conductivity is obtained (without any fitting parameters) from the data of Figures 7a and 7b; the resulting real part of the conductivity is shown in Figure 7c and the imaginary part in Figure 7d. The real part is strongly frequency dependent, dropping monotonically from its DC peak to a reduced value at the highest measured frequency of 2 THz. The extrapolated DC conductivities are 0.89 Ωcm for the P-type material and 1.13 Ωcm for the N-type, compared to the directly measured values of 0.92 Ωcm (P-type) and 1.15 Ωcm (N-type). The behavior of the imaginary part is completely different, increasing from zero at low frequencies, peaking at mid-range and then showing a gradual decline. The agreement with the Drude theory (solid line) is quite acceptable.

The two Drude parameters, the plasma angular frequency $\omega_p$ and the damping rate Γ, were determined within

5% accuracy from the fits to the data. For 0.92 Ωcm P-type silicon, $\omega_p/2\pi$ = 1.75 THz and $\Gamma/2\pi$ = 1.51 THz, while for 1.15 Ωcm N-type silicon, $\omega_p/2\pi$ = 1.01 THz and $\Gamma/2\pi$ = 0.64 THz. The measured damping rates and the known effective carrier masses[28] determine mobilities of 1680 $cm^2/Vs$ for the electrons and 500 $cm^2/Vs$ for the holes. The measured plasma frequencies and effective carrier masses determine the carrier densities of $1.4 \times 10^{16} cm^{-3}$ for the P-type and $3.3 \times 10^{15} cm^{-3}$ for the N-type silicon. Thus, these device-grade silicon wafers have been electrically characterized from low frequencies to 2 THz by THz-TDS.

## Some Recent Work

An unusual and interesting observation was that after excitation by a well-collimated beam of subpsec pulses of THz radiation, an $N_2O$ vapor cell emitted a coherent THz pulse train extending to as long as 1 nsec.[29] The individual subpsec THz pulses of the train were separated by 39.8 psec, corresponding to the frequency separation between adjacent rotational lines of the excited manifold of more than 50 lines. From the decay of the pulse train, the coherent relaxation time $T_2$ was obtained as a function of vapor pressure, even for the case of overlapping lines. In addition, the frequency separation between the rotational lines was determined from the pulse repetition rate in the train. Finally, from the changing individual pulse shapes in the train the anharmonicity factor for the $N_2O$ molecule was evaluated.

High-$T_c$ superconducting films have been studied by THz time-domain spectroscopy.[34-36] From the amplitude and phase changes of the subpsec pulses of THz radiation transmitted through the films, the complex conductivity[34] and the real and imaginary parts of the surface impedance[35] were measured in both the normal and superconducting states. In other work,[36] where the real and imaginary parts of the sub-band-gap conductivity $\sigma$ of $YBa_2Cu_3O_7$ films were directly measured in the frequency range from 15-80 $cm^{-1}$, a peak was observed in the real part $\sigma_1$ similar to the coherence peak expected in an s-wave BCS superconductor. The fact that this peak is absent in NMR relaxation-rate experiments suggests that its origin lies in a strongly temperature-dependent inelastic-scattering rate rather than in coherence factors.


## Acknowledgments

This work would not have been possible without the excellent masks and wafer fabrication by Hoi Chan. It has been my pleasure to have worked with the following outstanding scientists in my group for various lengths of time, while we developed the optoelectronic teraHz beam system described in this review and demonstrated its usefulness for THz time-domain-spectroscopy. The individuals are: Christof Fattinger (1987-1989), Martin van Exter (1988-1989), Søren R. Keiding (1989-1990), Hermann Harde (1990), Nir Katzenellenbogen (1990-), Stephen E. Ralph (1990-). It is my honor to be able to describe their many accomplishments.


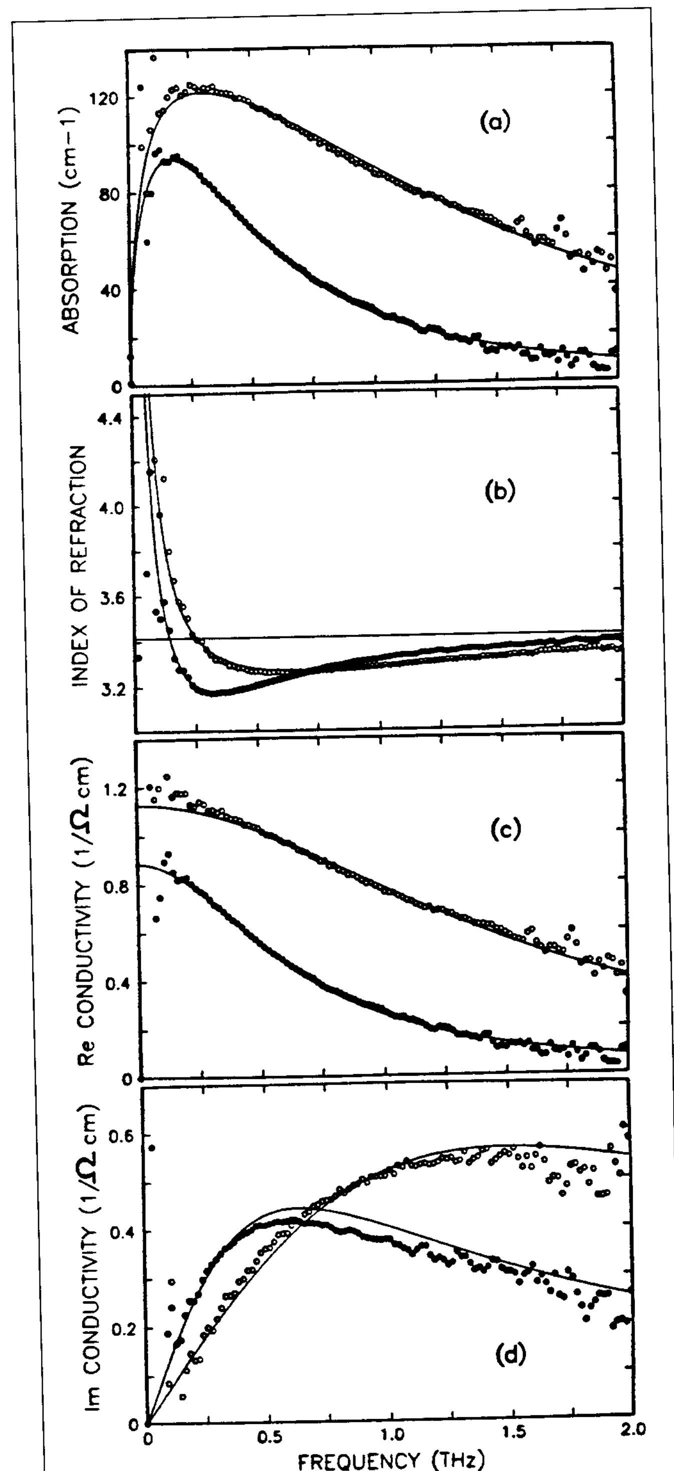


Figure 7. TDS results to 2 THz for 1.15 Ωcm, N-type (dots, lower curves) and 0.92 Ωcm, P-type (circles) silicon. (a) Power absorption. (b) Index of refraction. (c) Real part of the electric conductivity. (d) Imaginary part of the electric conductivity.

**D. GRISCHKOWSKY** *is manager of the Ultrafast Science with Lasers Group at the IBM T.J. Watson Research Center in Yorktown Heights, N.Y.*

## REFERENCES


1. D.H. Auston *et al.*, "Picosecond photoconducting Hertzian dipoles," Appl. Phys. Lett. **45**, 1984, 284-286.
2. C. Fattinger and D. Grischkowsky, "Point source terahertz optics," Appl. Phys. Lett. **53**, 1988, 1480; "TeraHz beams," **54**, 1989, 490-492.
3. G. Mourou *et al.*, "Picosecond microwave pulses generated with a subpicosecond laser-driven semiconductor switch," Appl. Phys. Lett. **39**, 1981, 295.
4. R. Heidemann *et al.*, "Optoelectronically pulsed slot-line antennas," Electron. Lett. **19**, 1983, 316-317.
5. A.P. DeFonzo *et al.*, "Transient response of planar integrated optoelectronic antennas," Appl. Phys. Lett. **50**, 1987, 1155; **51**, 1987, 212-214.
6. Y. Pastol *et al.*, "Characterization of an optoelectronically pulsed broadband microwave antenna," Electron. Lett. **24**, 1988, 1318-1319.
7. P.R. Smith *et al.*, "Subpicosecond photoconducting dipole antennas," IEEE J. Quantum Elect. **24**, 1988, 255-260.
8. M. van Exter *et al.*, "High brightness teraHz beams characterized with an ultrafast detector," Appl. Phys. Lett. **55**, 1989, 337-339.
9. Y. Pastol *et al.*, "Characterization of an optoelectronically pulsed equiangular spiral antenna," Electron. Lett. **26**, 1990, 133-134.
10. M. van Exter and D. Grischkowsky, "Characterization of an optoelectronic teraHz beam system," IEEE Trans. Microwave Theory Tech. **38**, 1990, 1684-1691.
11. D.R. Dykaar *et al.*, "Log-periodic antennas for pulsed terahertz radiation," Appl. Phys. Lett. **59**, 1991, 262-254.
12. D.H. Auston, "Subpicosecond electro-optic shockwaves," Appl. Phys. Lett. **43**, 1983, 713-715.
13. B.B. Hu *et al.*, "Free-space radiation from electro-optic crystals," Appl. Phys. Lett. **56**, 1990, 506-508.
14. D. Grischkowsky *et al.*, "Electromagnetic shock waves from transmission lines," Phys. Rev. Lett. **59**, 1987, 1663-1666.
15. C. Fattinger and D. Grischkowsky, "A Cherenkov source for freely propagating teraHz beams," IEEE J. Quantum Electron. **QE-25**, 1989, 2608-2610.
16. X.C. Zhang *et al.*, "Generation of femtosecond electromagnetic pulses from semiconductor surfaces," Appl. Phys. Lett. **56**, 1990, 1011-1013.
17. X.C. Zhang *et al.*, "Optically induced electromagnetic radiation from semiconductor surfaces," Appl. Phys. Lett. **56**, 1990, 2228-2230.
18. X.C. Zhang *et al.*, "Optically induced femtosecond electromagnetic pulses from GaSb/AlSb strained-layer superlattices," Appl. Phys. Lett. **57**, 1990, 753-755.
19. L. Xu *et al.*, "Terahertz radiation from large aperture Si p-i-n diodes," Appl. Phys. Lett. **59**, 1991, 3357-3359.
20. N. Katzenellenbogen and D. Grischkowsky, "Efficient generation of 380 fs pulses of THz radiation by ultrafast laser pulse excitation of a biased metal-semiconductor interface," Appl. Phys. Lett. **58**, 1991, 222-224.
21. S.E. Ralph and D. Grischkowsky, "Trap-enhanced electric fields in semi-insulators: The role of electrical and optical carrier injection, "Appl. Phys. Lett, **59** 1991, 1972-1974.
22. D. Grischkowsky and N. Katzenellenbogen, "Femtosecond pulses of terahertz radiation: Physics and applications," OSA Proc. on Psec. Elect. and Optoelect. **9**, T.C.L. Gerhard Sollner and Jagdeep Shah, eds., Optical Society of America, Washington, D.C.. 1991).
23. B.I. Greene *et al.*, "Interferometric characterization of 160 fs far-infrared light pulses," Appl. Phys. Lett. **59**, 1991, 893-895.
24. S.E. Ralph and D. Grischkowsky, "THz spectroscopy and source characterization by optoelectronic interferometry," Appl. Phys. Lett. **60**, 1992, 1070-1072.
25. A.C. Warren *et al.*, "Arsenic precipitates and the semi-insulating properties of GaAs buffer layers grown by low-temperature molecular beam epitaxy," Appl. Phys. Lett. **57**, 1990, 1331-1333.
26. A.C. Warren *et al.*, "Subpicosecond, freely propagating electromagnetic pulse generation and detection using GaAs:As epilayers," Appl. Phys. Lett. **58**, 1991, 1512-1514.
27. D. Grischkowsky *et al.*, "Far-infrared time-domain spectroscopy with terahertz beams of dielectrics and semiconductors," J. Opt. Soc. Am. B **7**, 1990, 2006-2015. This paper contains a discussion and an extensive reference list describing the development of time-domain-spectroscopy.
28. M. van Exter and D. Grischkowsky, "Optical and electronic properties of doped silicon from 0.1 to 2 THz," Appl. Phys. Lett. **56**, 1990, 1694; "Carrier dynamics of electrons and holes in moderately doped silicon," Phys. Rev. B15 **41**, 1990, 12140-12149.
29. H. Harde *et al.*, "THz commensurate echoes: Periodic rephasing of molecular transitions in free-induction decay," Phys. Rev. Lett. **66**, 1991, 1834-1837; H. Harde and D. Grischkowsky, J. Opt. Soc. Am. B **8**, 1991, 1642-1651.
30. Martin van Exter *et al.*, "Terahertz time-domain spectroscopy of water vapor," Optics Lett. **14**, 1989, 1128-1130.
31. *American Institute of Physics Handbook*, third edition, D.E. Gray, ed., McGraw-Hill Book Co., New York, N.Y., reissued and published 1982.
32. E.E. Russell and E.E. Bell, "Optical constants of sapphire in the far-infrared," J. Opt. Soc. Am. **57**, 1967, 543-544.
33. E.V. Loewenstein *et al.*, "Optical constants of far-infrared materials," Appl. Opt. **12**, 1973, 398-406.
34. J.M. Chwalek *et al.*, "Submillimetre wave response of superconducting $YBa_2Cu_30_{7-x}$ using coherent time-domain spectroscopy," Electron. Lett. **27**, 1991, 447.
35. M.C. Nuss *et al.*, "Terahertz surface impedance of thin $YBa_2Cu_3O_7$ superconducting films," Appl. Phys. Lett., **58**, 1991, 2561.
36. M.C. Nuss *et al.*, "Dynamic conductivity and `coherence peak' in $YBa_2Cu_3O_7$ superconductors," Phys. Rev. Lett. **66**, 1991, 3305.